

## Fragile Topology and Flat-Band Superconductivity in the Strong-Coupling Regime

Valerio Peri<sup>1,\*</sup>, Zhi-Da Song,<sup>2</sup> B. Andrei Bernevig,<sup>2</sup> and Sebastian D. Huber<sup>1</sup>

<sup>1</sup>*Institute for Theoretical Physics, ETH Zurich, 8093 Zürich, Switzerland*

<sup>2</sup>*Department of Physics, Princeton University, Princeton, New Jersey 08544, USA*



(Received 6 August 2020; accepted 11 December 2020; published 14 January 2021)

In flat bands, superconductivity can lead to surprising transport effects. The superfluid “mobility”, in the form of the superfluid weight  $D_s$ , does not draw from the curvature of the band but has a purely band-geometric origin. In a mean-field description, a nonzero Chern number or fragile topology sets a lower bound for  $D_s$ , which, via the Berezinskii-Kosterlitz-Thouless mechanism, might explain the relatively high superconducting transition temperature measured in magic-angle twisted bilayer graphene (MATBG). For fragile topology, relevant for the bilayer system, the fate of this bound for finite temperature and beyond the mean-field approximation remained, however, unclear. Here, we numerically use exact Monte Carlo simulations to study an attractive Hubbard model in flat bands with topological properties akin to those of MATBG. We find a superconducting phase transition with a critical temperature that scales linearly with the interaction strength. Then, we investigate the robustness of the superconducting state to the addition of trivial bands that may or may not trivialize the fragile topology. Our results substantiate the validity of the topological bound beyond the mean-field regime and further stress the importance of fragile topology for flat-band superconductivity.

DOI: 10.1103/PhysRevLett.126.027002

Whenever the single particle’s kinetic energy does not depend on momentum, noninteracting electrons, if not in a topological state, are strictly localized. Nevertheless, these seemingly inert systems exhibit intriguing transport phenomena in the presence of many-body effects. A paradigmatic example is the onset of unconventional superconductivity, where mobile coherent electron pairs emerge from an insulating high-temperature state [1–12] under the influence of strong electron-electron interactions. The interest in this flat-band superconductivity surged after its observation in magic-angle twisted bilayer graphene (MATBG) [13]. Since then, signatures of zero-resistance states have been reported in other flat-band van der Waals systems such as twisted double-bilayer graphene [14–16], twisted trilayer graphene [17], ABC–trilayer graphene [18], and bilayer WSe<sub>2</sub> [19].

Superconductivity arises from the interplay of two different energy scales: the effective electron-electron attractive interaction  $|U|$  and the bandwidth  $W$ . A vanishing bandwidth maximizes the density of states  $n_0(\epsilon_F)$  at the Fermi energy and the Bardeen-Cooper-Schrieffer (BCS) theory predicts  $T_{c,\text{BCS}} \propto |U|n_0(\epsilon_F)$  in the flat-band limit  $|U| \gg W$  [1–3]. While the BCS theory might seem unsuitable to treat systems lacking a well-defined Fermi surface, the BCS wave function turns out to be an exact zero-temperature ground state for certain flat bands with local attractive interactions [5,20]. Nevertheless, the validity of the BCS theory at finite temperature is questionable and one needs to be careful in exploring the strong-coupling regime [21,22]. Moreover, while the BCS theory

captures the formation of electronic pairs, their phase fluctuations are known to be crucial in two-dimensional (2D) superconductors [23].

Phase coherence emerges via the Berezinskii-Kosterlitz-Thouless (BKT) mechanism [24–26]. Within the BKT theory, the fraction of electrons condensed into coherent bound pairs is captured by the superfluid weight  $D_s(T)$ . The universal jump in this quantity determines the transition temperature  $T_c$ :  $T_c = \pi D_s^- / 2$ , where  $D_s^-$  is the superfluid weight at the critical temperature approached from below [27].

The Ginzburg-Landau theory for conventional superconductors predicts  $D_s(T=0) \approx e^2 n_s / m^*$ , where  $n_s$  is the amplitude of the superconducting order parameter, and  $m^*$  is the effective band mass [28]. Exactly flat bands have an infinite effective mass,  $m^* = \infty$ . Hence, a vanishing bandwidth seems detrimental to phase coherence. Therefore, one would expect phase fluctuations to completely disrupt superconductivity in dispersionless bands. However, this conclusion neglects other band properties that are not captured by a simple effective mass approximation.

The presence of a further contribution to the superfluid weight is now well established in the mean-field approximation [5,20,29,30]. This additional term has a band-geometric origin and is proportional to the Fubini-Study metric of the occupied bands [20]. Lower bounds for  $D_s(T=0)$  have been formulated both for bands with a nonzero Chern number [20] as well as for two bands characterized by fragile topology [31].

While the bound in terms of the Chern number and its influence on the  $T \neq 0$  physics has been recently investigated numerically in the strong-coupling regime [21], no such analysis has been performed for the case of fragile topology. The latter is particularly relevant since the single-particle nearly flat bands of MATBG have zero Chern number but nontrivial fragile topology [32–37]. In the current Letter, we fill this gap by studying a concrete flat-band model with fragile topology via exact numerical methods.

First, we review the concept of fragile topological bands and introduce the concrete model used in this Letter. Then, we compare the superfluid weight obtained from quantum Monte Carlo simulations to the zero-temperature mean-field topological bound. To further establish the importance of fragile topology, we investigate the fate of the superconducting state under the addition of trivial bands. Finally, we analyze the properties of the normal state above the superconducting phase transition.

Fragile Bloch bands represent a flavor of symmetry protected topological insulators (TIs), as these bands cannot be represented by translationally and lattice temporal-spatial symmetric, exponentially localized Wannier functions. However, the addition of a trivial Bloch band can resolve this obstruction, contrary to the stable TIs [36,38–41]. In the case of MATBG, the protecting symmetry is  $C_{2z}\mathcal{T}$ , where  $C_{2z}$  is a  $180^\circ$  rotation around the out-of-plane axis  $\hat{z}$ , and  $\mathcal{T}$  is the bosonic time-reversal symmetry that acts as complex conjugation. For two occupied bands with  $C_{2z}\mathcal{T}$  symmetry, it is possible to introduce a  $\mathbb{Z}$  classification based on the Euler class,  $e_2$ , of real orientable bundles [31,35,36,39,42]. In particular, Ref. [31] showed that, in the mean-field approximation, a nontrivial Euler class provides a lower bound on  $D_s(T=0)$ . The geometric contribution to the superfluid weight of MATBG has, since then, been discussed further in [31,43,44].

To investigate the robustness of the bound for fragile bands in the strong-coupling regime, we follow Ref. [21] and consider an attractive Hubbard model which lends itself to numerically exact auxiliary-field quantum Monte Carlo simulations [45–47].

We focus on a particular 2D lattice model, known as kagome-3 [48–50], which represents a minimal instance of a flat-band system characterized by fragile topology. The lattice, its basis vectors  $\mathbf{a}_1 = (1, 0)$  and  $\mathbf{a}_2 = (1/2, \sqrt{3}/2)$ , and the three inequivalent sublattices in the unit cell are shown in Fig. 1(a). We study the Hamiltonian

$$H = H_{\text{kin}} + H_{\text{int}}, \quad (1)$$

$$H_{\text{kin}} = \sum_{i,j,\sigma} t_{ij} c_{i\sigma}^\dagger c_{j\sigma} - \mu \sum_i (n_{i\downarrow} + n_{i\uparrow}), \quad (2)$$

$$H_{\text{int}} = -|U| \sum_i \left( n_{i\uparrow} - \frac{1}{2} \right) \left( n_{i\downarrow} - \frac{1}{2} \right), \quad (3)$$

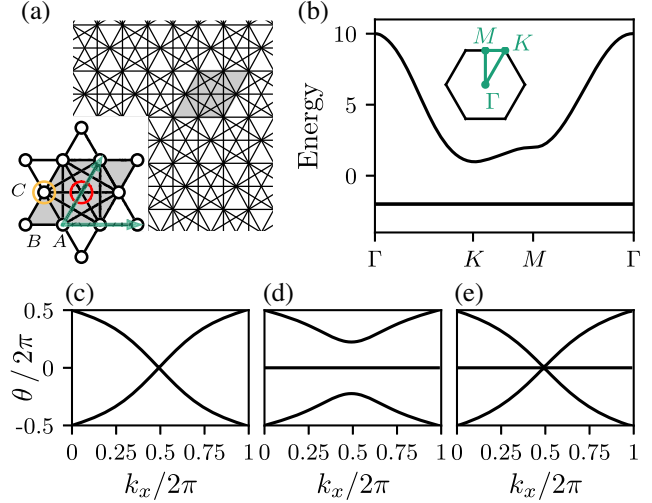


FIG. 1. (a) Kagome-3 lattice model with the unit-cell area shaded in gray. The inset shows the details of one plaquette. The red circle highlights the  $1a$  Wyckoff position of the lattice, while the yellow circle the  $1b$  Wyckoff position. Note that, although the full point group of the model is  $p6mm$ , we refer to the real space high-symmetry points of its subgroup  $p2$  [51]. The basis vectors  $\mathbf{a}_1$  and  $\mathbf{a}_2$  are represented by the green arrows. The three inequivalent sublattices  $A$ ,  $B$ , and  $C$  are also highlighted. (b) Single-particle spectrum of the model along high-symmetry lines of  $p6mm$ . The high-symmetry lines and the first Brillouin zone (BZ) are shown in the inset. The flat bands at  $\epsilon = -2$  are doubly degenerate. (c) Wilson loop spectrum of the two flat bands of the kagome-3 model. (d) Wilson loop spectrum of the three lowest bands of the model with an additional  $s$  orbital at  $1a$  Wyckoff position. (e) Same as (d) but with an  $s$  orbital at  $1b$  Wyckoff position.

where  $c_{i\sigma}$  is the fermionic annihilation operator, and  $n_{i\sigma} = c_{i\sigma}^\dagger c_{i\sigma}$  counts the number of electrons on site  $i$  with spin  $\sigma = \{\uparrow, \downarrow\}$ .  $|U|$  is the electron-electron interaction strength,  $\mu$  the chemical potential, and  $t_{ij}$  the hopping parameter between sites  $i$  and  $j$ . In the remainder, we set all hopping terms to unity.

The single-particle physics encoded in Eq. (2) is particularly appealing. The spectrum of the model has two degenerate flat bands at  $\epsilon(\mathbf{k}) = -2$  and a third dispersive band  $\epsilon(\mathbf{k}) = 4 + 2[\cos \mathbf{k} \cdot \mathbf{a}_1 + \cos \mathbf{k} \cdot \mathbf{a}_2 + \cos \mathbf{k} \cdot (\mathbf{a}_1 - \mathbf{a}_2)]$ , cf. Fig. 1(b). The smallest gap  $\delta = 3$  between the dispersive and flat bands is attained at the momentum point  $K = (2\pi/3, 2\pi/\sqrt{3})$  [51]. Note that the model possesses both spinful time-reversal symmetry and spin  $S^z$  conservation. These features allow us to study the topological properties by computing the Wilson loop operators of each spin sector independently [20,31,51]. As shown in Fig. 1(c), the winding in the Wilson loop spectra of the two flat bands establishes their topological nature with a nontrivial Euler class  $|e_2| = 1$  protected by  $C_{2z}\mathcal{T}$  [36,39,51]. The winding of the spectrum is removed by the addition of a trivial band, as shown in Fig. 1(d), confirming the presence of fragile topology. Thus, the

topological properties of the kagome-3 flat bands are akin to those of the single-particle bands of MATBG [32–37].

To compute  $D_s(T)$ , we introduce an external electromagnetic field via its electromagnetic potential  $\mathbf{A}$  and Peierls substitution:  $t_{ij} \rightarrow t_{ij} \exp[i\mathbf{A} \cdot (\mathbf{r}_i - \mathbf{r}_j)] = t_{ij}(\mathbf{r})$ , where  $\mathbf{r}_i$  is the position of the site  $i$  and  $\mathbf{r} = \mathbf{r}_i - \mathbf{r}_j$ . Then, we can expand  $H(\mathbf{A})$  up to second order in  $\mathbf{A}$

$$H(\mathbf{A}) = H + j_\mu^p A_\mu + \frac{1}{2} T_{\mu\nu} A_\mu A_\nu, \quad (4)$$

where  $j_\mu^p$  is the paramagnetic current operator and  $T_{\mu\nu} A_\nu$  is the diamagnetic one. These operators are defined as

$$j_\mu^p = \sum_{ij,\sigma} \frac{\partial t_{ij}(\mathbf{r})}{\partial r_\mu} c_{i\sigma}^\dagger c_{j\sigma}, \quad (5)$$

and

$$T_{\mu\nu} = \sum_{ij,\sigma} \frac{\partial^2 t_{ij}(\mathbf{r})}{\partial r_\mu \partial r_\nu} c_{i\sigma}^\dagger c_{j\sigma}. \quad (6)$$

The superfluid weight characterizes the zero-frequency, long-wavelength response to the external field,  $j_\mu = D_{s,\mu\nu} A_\nu$ . It is given by

$$D_{s,\mu\nu} = \frac{1}{4} [\langle T_{\mu\nu} \rangle - \Lambda_{\mu\nu}(k_{\parallel} = 0, k_{\perp} \rightarrow 0, i\omega_m = 0)], \quad (7)$$

where  $k_{\parallel(\perp)}$  is the momentum component parallel (perpendicular) to  $\mathbf{A}$ , and  $\langle \cdot \rangle$  represents the expectation value over the many-body ground state of Eq. (1) at temperature  $T$ . Here,  $\Lambda_{\mu\nu}(\mathbf{k}, \omega)$  is the current-current correlator

$$\Lambda_{\mu\nu}(\mathbf{k}, i\omega_m) = \int_0^\beta d\tau e^{i\omega_m \tau} \langle [j_\mu^p(\mathbf{k}, \tau), j_\nu^p(-\mathbf{k}, 0)] \rangle, \quad (8)$$

with  $\omega_m = 2\pi mT$ ,  $m \in \mathbb{Z}$ , and  $\beta = 1/k_B T$  the inverse temperature. In the remainder, we consider  $D_s = D_{s,xx}$  and a gauge potential  $\mathbf{A} = A\hat{\mathbf{x}}$ .

The quantum Monte Carlo simulations grant access to the superfluid weight  $D_s(T)$  in the strong-coupling regime at finite temperature [51]. We perform simulations in the grand canonical ensemble, where the chemical potential  $\mu$  controls the filling  $\nu$  of the system. We carefully tune  $\mu(T)$  to ensure  $\nu = 1/3$ , i.e., two electrons per unit cell and half-filling of the flat bands. We focus on a range of Hubbard interactions  $|U| < \delta$ , where  $\delta$  is the energy gap between the flat bands and the dispersive one.

First, we consider  $|U| = 2$  and lattices of different sizes  $L \times L$ , with  $L = 4, 6, 8$ . Since each unit cell contains three inequivalent sublattices and we consider spinful electrons, the number of orbitals in these systems is 96, 216, 384, respectively. In Fig. 2(a), we present the results of this analysis. The transition temperature  $T_c/|U| \approx 0.02$  is given by the universal jump in the superfluid weight  $D_s(T)$  [27] and shows little dependence on the system's size.

Next, we investigate the relation between  $T_c$  and  $|U|$ . Since the Hubbard interaction is the only energy scale of the problem, we expect a linear relation between  $T_c$  and  $|U|$ :  $T_c \propto |U|$  [20]. This observation is confirmed by the plot of  $D_s(T/|U|)/|U|$  with  $|U| = 1, 1.5, 2$  for a  $6 \times 6$  system. The three curves lie on top of each other and confirm  $T_c/|U| \approx 0.02$ , cf. Fig. 2(b). These findings parallel those for flat Chern bands in the strong-coupling regime [21] and substantiate the onset of superconductivity in the exactly flat bands of the kagome-3 lattice.

The addition of trivial bands to a fragile topological insulator can remove the obstruction to an atomic limit and might impact the strength of the superconducting order. Therefore, we carefully assess the fate of superconductivity when further bands are considered.

To investigate the Wannierizability under the addition of trivial bands, we resort to an analysis of the symmetry eigenvalues of  $C_{2z}$  [51]. This approach allows us to consider two different scenarios. First, we couple an extra  $s$  orbital at the  $1a$  Wyckoff position [red circle in Fig. 1(a)] to all adjacent sites. This additional orbital gives rise to an

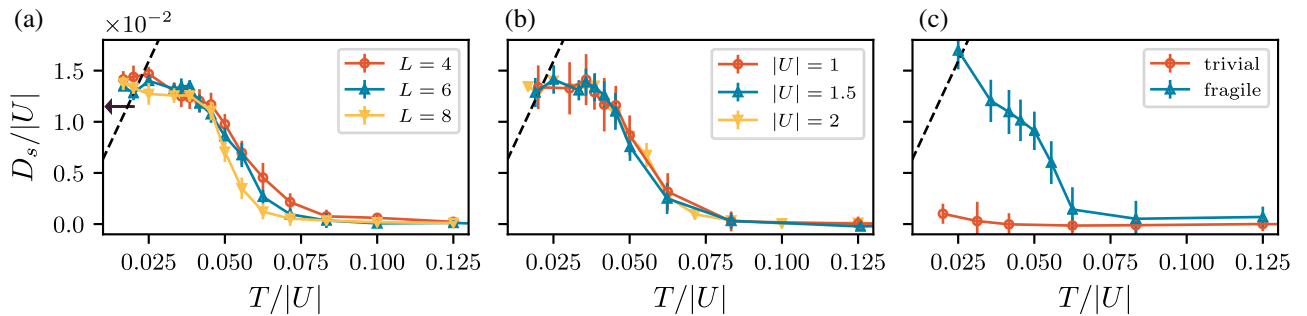


FIG. 2. Superfluid weight  $D_s(T)$  for the attractive Hubbard model with interaction strength  $|U|$ . The crossing of  $D_s$  with the dashed line  $2T/\pi$  indicates the BKT transition, where the superconducting transition occurs. (a) Different system sizes  $L \times L$ , with  $L = 4, 6, 8$  and  $|U| = 2$ . The arrow on the y axis represents the mean-field topological lower bound for  $D_s(T = 0)$  [51]. (b) Different interaction strengths  $|U| = 1, 1.5, 2$  in a  $6 \times 6$  system. In both (a) and (b) the kagome-3 model is considered. (c) Results for the four-band models for  $|U| = 2$  and  $L = 6$ . The trivial model has an additional  $s$  orbital at Wyckoff position  $1a$ , cf. Fig. 1(a). The model with fragile topology has an additional  $s$  orbital at Wyckoff position  $1b$ , instead, cf. Fig. 1(a).

$A_{1a}$  band that trivializes the flat bands of the original model, see [51] for a detailed analysis. A fine-tuning of the on site energy of the added site results in a four-band model with three exactly flat bands for arbitrary hopping strength to the additional site. Second, we add a  $s$  orbital at  $1b$  Wyckoff position [yellow circle in Fig. 1(a)]. Note that we always consider only the subgroup  $p2$  of the full point group  $p6mm$  of the original kagome-3 model [51]. This additional orbital gives rise to an  $A_{1b}$  band that does not remove the obstruction to an atomic limit. The nontrivial topology is now protected by  $C_{2z}$  rather than  $C_{2z}\mathcal{T}$  [51]. In this second case, it is not possible to achieve three exactly flat bands with finite range hopping. However, the addition of longer range hopping allows us to obtain three bands with  $W/\delta \approx 0.03$  and a coupling strength to the addition site comparable to the first case. The different topological properties of these models can be read off the respective Wilson loop spectra [65] of Figs. 1(d)–1(e): winding spectrum for the topological case, gapped for the trivial one.

In the Monte Carlo simulations of these four-band models, we tune  $\mu$  to achieve a filling  $\nu = 3/8$ . This value corresponds to the half-filling of the lower three bands, where we intend to study the influence of fragile topology on the superconducting behavior. The evolution of the superfluid weight as a function of temperature confirms the important role played by fragile topology, as can be seen in Fig. 2(c). In the topologically trivial model,  $D_s(T)$  remains zero down to temperatures below the critical temperature of the original three-band model. On the other hand, the model with fragile topology protected by  $C_{2z}$  symmetry behaves similarly to the kagome-3 model.

For completeness, we now turn our attention to the physics above the superconducting transition in the kagome-3 lattice. First, we study the spin susceptibility

$$\chi_S = \frac{1}{L^2} \int_0^\beta d\tau \langle S^z(\tau) S^z(0) \rangle, \quad (9)$$

with  $S^z = \sum_i (c_{i\uparrow}^\dagger c_{i\uparrow} - c_{i\downarrow}^\dagger c_{i\downarrow})$  [51]. As shown in Fig. 3(a), it reaches a maximum at  $T_S/|U| \approx 0.17$ . This result points to the onset of singlet formation already above  $T_c$  [66].

Next, we investigate the single-particle density of states [51,67]

$$N(\epsilon_F) = \frac{\beta}{\pi L^2} \sum_\alpha \int_{\text{BZ}} d\mathbf{k} \langle c_{\alpha\mathbf{k}}(\beta/2) c_{\alpha\mathbf{k}}^\dagger(0) \rangle, \quad (10)$$

where  $\alpha$  is the sublattice index.  $N(\epsilon_F)$  peaks at temperature  $T_N/|U| \approx 0.09$  and drops toward zero at lower temperatures, cf. Fig. 3(b). The temperature range  $T_c < T < T_N$ , where the opening of a gap reduces the density of states before the system turns superconducting, is associated with a pseudogap regime characterized by strong phase

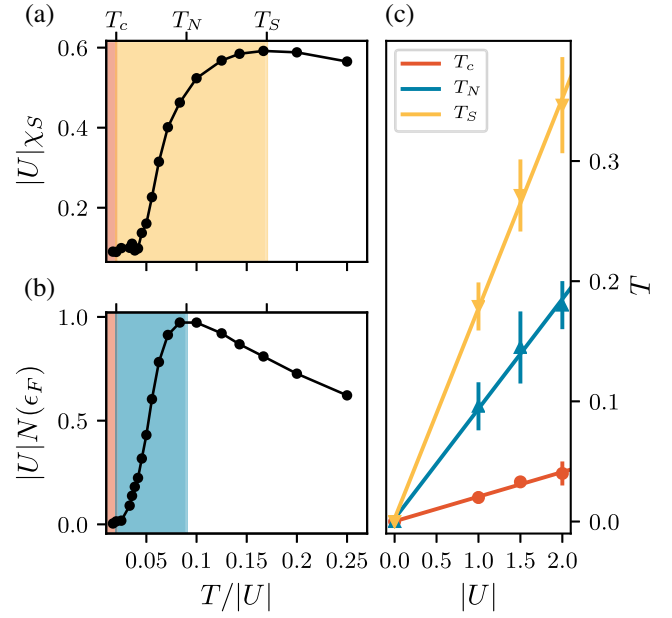


FIG. 3. (a) Spin susceptibility  $\chi_S$  as a function of temperature  $T$  for the Hubbard model on the kagome-3 lattice with  $|U| = 2$  and  $L = 6$ . (b) Single-particle density of states  $N(\epsilon_F)$  as a function of temperature  $T$  for the same model. The shaded areas correspond to the superconducting state in dark orange, the range below  $\chi_S$  peaks in yellow and that below the peak of  $N(\epsilon_F)$  in blue. (c) Scaling of the critical temperatures  $T_c$ ,  $T_S$ , and  $T_N$  as a function of the interaction strength  $|U|$ . All these quantities show a linear scaling.

fluctuations [68]. Note that, for  $T < T_N$ , the spin susceptibility  $\chi_S$  also gets significantly suppressed.

Our results establish the importance of nontrivial fragile topology for the onset of superconductivity in flat bands. In summary, the signatures of a single-particle gap above the critical temperature are typical for attractive Hubbard models in the strong-coupling regime [67]. Moreover, the linear scaling with  $|U|$  of the characteristic temperatures  $T_c$ ,  $T_S$ , and  $T_N$  shown in Fig. 3(c) is a generic feature of flat band physics for  $|U| < \delta$  [3,21]. In particular, the pseudogap temperature scales linearly with  $|U|$  regardless of whether it is identified with  $T_S$  [66] or  $T_N$ . Beyond these results, it was recently shown that band topology can play a crucial role in the strength of superconductivity [21,22]. While the authors of Ref. [21] considered the case of a Chern number, in our Letter, the topological invariant ensuring a high critical temperature is a fragile one relevant for a broad class of time reversal invariant systems. In particular, we prove how this new protecting mechanism is robust beyond the mean-field approximation of Ref. [31] but has important consequences for the fate of the superconducting state under the addition of trivial bands. Especially in two-dimensional systems, such additional bands naturally arise in tunnel-coupled heterostructures. This direct link between fragility and an observable quantity is an important step forward in our understanding

of fragile topological insulators which have only a handful of known experimental signatures [32,33,69–72]. Despite the infancy of this field, there is evidence that a myriad of materials and engineered structures possess this peculiar topology [73–76], calling for further studies of interactions in fragile bands [41,71,77].

This work was supported by a grant from the Swiss National Supercomputing Centre (CSCS) under Project ID No. eth5b. The auxiliary-field QMC simulations were carried out with the ALF package. V.P., and S.D.H. acknowledge support from the Swiss National Science Foundation, the NCCR QSIT, and the European Research Council under the Grant Agreement No. 771503 (TopMechMat). Z.S. and B.A.B. are supported by the U.S. Department of Energy Grant No. DE-SC0016239, the Schmidt Fund for Innovative Research, Simons Investigator Grant No. 404513, the Packard Foundation, the National Science Foundation EAGER Grant No. DMR-1643312, NSF-MRSEC Grant No. DMR-1420541, BSF Israel US foundation Grant No. 2018226, ONR Grant No. N00014-20-1-2303, and the Princeton Global Network Funds.

\*periv@phys.ethz.ch

- [1] V. A. Khodel' and V. R. Shaginyan, *JETP Lett.* **51**, 553 (1990).
- [2] N. B. Kopnin, T. T. Heikkilä, and G. E. Volovik, *Phys. Rev. B* **83**, 220503(R) (2011).
- [3] G. E. Volovik, *J. Supercond. Novel Magn.* **26**, 2887 (2013).
- [4] V. I. Iglovikov, F. Hébert, B. Grémaud, G. G. Batrouni, and R. T. Scalettar, *Phys. Rev. B* **90**, 094506 (2014).
- [5] M. Tovmasyan, S. Peotta, P. Törmä, and S. D. Huber, *Phys. Rev. B* **94**, 245149 (2016).
- [6] V. J. Kauppila, F. Aikebaier, and T. T. Heikkilä, *Phys. Rev. B* **93**, 214505 (2016).
- [7] K. Kobayashi, M. Okumura, S. Yamada, M. Machida, and H. Aoki, *Phys. Rev. B* **94**, 214501 (2016).
- [8] T. Löthman and A. M. Black-Schaffer, *Phys. Rev. B* **96**, 064505 (2017).
- [9] R. Ojajarvi, T. Hyart, M. A. Silaev, and T. T. Heikkilä, *Phys. Rev. B* **98**, 054515 (2018).
- [10] P. Kumar, T. I. Vanhala, and P. Törmä, *Phys. Rev. B* **100**, 125141 (2019).
- [11] L. H. C. M. Nunes and C. M. Smith, *Phys. Rev. B* **101**, 224514 (2020).
- [12] N. Swain and M. Karmakar, *Phys. Rev. Research* **2**, 023136 (2020).
- [13] Y. Cao, V. Fatemi, S. Fang, K. Watanabe, T. Taniguchi, E. Kaxiras, and P. Jarillo-Herrero, *Nature (London)* **556**, 43 (2018).
- [14] C. Shen, Y. Chu, Q. Wu, N. Li, S. Wang, Y. Zhao, J. Tang, J. Liu, J. Tian, K. Watanabe, T. Taniguchi, R. Yang, Z. Y. Meng, D. Shi, O. V. Yazyev, and G. Zhang, *Nat. Phys.* **16**, 520 (2020).
- [15] Y. Cao, D. Rodan-Legrain, O. Rubies-Bigorda, J. M. Park, K. Watanabe, T. Taniguchi, and P. Jarillo-Herrero, *Nature (London)* **583**, 215 (2020).
- [16] X. Liu, Z. Hao, E. Khalaf, J. Y. Lee, Y. Ronen, H. Yoo, D. H. Najafabadi, K. Watanabe, T. Taniguchi, A. Vishwanath, and P. Kim, *Nature (London)* **583**, 221 (2020).
- [17] K.-T. Tsai, X. Zhang, Z. Zhu, Y. Luo, S. Carr, M. Luskin, E. Kaxiras, and K. Wang, *arXiv:1912.03375*.
- [18] G. Chen, A. L. Sharpe, P. Gallagher, I. T. Rosen, E. J. Fox, L. Jiang, B. Lyu, H. Li, K. Watanabe, T. Taniguchi, J. Jung, Z. Shi, D. Goldhaber-Gordon, Y. Zhang, and F. Wang, *Nature (London)* **572**, 215 (2019).
- [19] L. Wang, E.-M. Shih, A. Ghiotto, L. Xian, D. A. Rhodes, C. Tan, M. Claassen, D. M. Kennes, Y. Bai, B. Kim, K. Watanabe, T. Taniguchi, X. Zhu, J. Hone, A. Rubio, A. N. Pasupathy, and C. R. Dean, *Nat. Mater.* **19**, 861 (2020).
- [20] S. Peotta and P. Törmä, *Nat. Commun.* **6**, 8944 (2015).
- [21] J. S. Hofmann, E. Berg, and D. Chowdhury, *Phys. Rev. B* **102**, 201112(R) (2020).
- [22] Z. Wang, G. Chaudhary, Q. Chen, and K. Levin, *Phys. Rev. B* **102**, 184504 (2020).
- [23] V. J. Emery and S. A. Kivelson, *Nature (London)* **374**, 434 (1995).
- [24] J. M. Kosterlitz and D. J. Thouless, *J. Phys. C* **6**, 1181 (1973).
- [25] A. Moreo and D. J. Scalapino, *Phys. Rev. Lett.* **66**, 946 (1991).
- [26] F. F. Assaad, W. Hanke, and D. J. Scalapino, *Phys. Rev. B* **49**, 4327 (1994).
- [27] D. R. Nelson and J. M. Kosterlitz, *Phys. Rev. Lett.* **39**, 1201 (1977).
- [28] D. J. Scalapino, S. R. White, and S. C. Zhang, *Phys. Rev. Lett.* **68**, 2830 (1992).
- [29] A. Julku, S. Peotta, T. I. Vanhala, D.-H. Kim, and P. Törmä, *Phys. Rev. Lett.* **117**, 045303 (2016).
- [30] L. Liang, T. I. Vanhala, S. Peotta, T. Siro, A. Harju, and P. Törmä, *Phys. Rev. B* **95**, 024515 (2017).
- [31] F. Xie, Z. Song, B. Lian, and B. A. Bernevig, *Phys. Rev. Lett.* **124**, 167002 (2020).
- [32] X. Lu, B. Lian, G. Chaudhary, B. A. Piot, G. Romagnoli, K. Watanabe, T. Taniguchi, M. Poggio, A. H. MacDonald, B. A. Bernevig, and D. K. Efetov, *arXiv:2006.13963*.
- [33] B. Lian, F. Xie, and B. A. Bernevig, *Phys. Rev. B* **102**, 041402(R) (2020).
- [34] H. C. Po, L. Zou, T. Senthil, and A. Vishwanath, *Phys. Rev. B* **99**, 195455 (2019).
- [35] Z. Song, Z. Wang, W. Shi, G. Li, C. Fang, and B. A. Bernevig, *Phys. Rev. Lett.* **123**, 036401 (2019).
- [36] J. Ahn, S. Park, and B.-J. Yang, *Phys. Rev. X* **9**, 021013 (2019).
- [37] M. P. Zaletel and J. Y. Khoo, *arXiv:1901.01294*.
- [38] H. C. Po, H. Watanabe, and A. Vishwanath, *Phys. Rev. Lett.* **121**, 126402 (2018).
- [39] A. Bouhon, A. M. Black-Schaffer, and R.-J. Slager, *Phys. Rev. B* **100**, 195135 (2019).
- [40] B. Bradlyn, Z. Wang, J. Cano, and B. A. Bernevig, *Phys. Rev. B* **99**, 045140 (2019).
- [41] D. V. Else, H. C. Po, and H. Watanabe, *Phys. Rev. B* **99**, 125122 (2019).

- [42] A. Bouhon, T. c. v. Bzdušek, and R.-J. Slager, *Phys. Rev. B* **102**, 115135 (2020).
- [43] A. Julku, T. J. Peltonen, L. Liang, T. T. Heikkilä, and P. Törmä, *Phys. Rev. B* **101**, 060505(R) (2020).
- [44] X. Hu, T. Hyart, D. I. Pikulin, and E. Rossi, *Phys. Rev. Lett.* **123**, 237002 (2019).
- [45] J. E. Hirsch, *Phys. Rev. B* **28**, 4059(R) (1983).
- [46] R. Blankenbecler, D. J. Scalapino, and R. L. Sugar, *Phys. Rev. D* **24**, 2278 (1981).
- [47] M. Bercx, F. Goth, J. S. Hofmann, and F. F. Assaad, *SciPost Phys.* **3**, 013 (2017).
- [48] L. Balents, M. P. A. Fisher, and S. M. Girvin, *Phys. Rev. B* **65**, 224412 (2002).
- [49] D. L. Bergman, C. Wu, and L. Balents, *Phys. Rev. B* **78**, 125104 (2008).
- [50] J.-W. Rhim and B.-J. Yang, *Phys. Rev. B* **99**, 045107 (2019).
- [51] See Supplemental Material at <http://link.aps.org/supplemental/10.1103/PhysRevLett.126.027002> for further details on the tight-binding models, the symmetry eigenvalues analysis, the calculations of the Wilson loop operators, the mean-field calculation of  $D_s$ , the auxiliary-field quantum Monte Carlo method, and additional characterization of the normal and superconducting states, e.g., the effect of nearest-neighbor interactions and  $|U| > \delta$ , which includes Refs. [52–64].
- [52] F. Wilczek and A. Zee, *Phys. Rev. Lett.* **52**, 2111 (1984).
- [53] J. Zak, *Phys. Rev. Lett.* **62**, 2747 (1989).
- [54] J. Ahn, D. Kim, Y. Kim, and B.-J. Yang, *Phys. Rev. Lett.* **121**, 106403 (2018).
- [55] J. Ahn, S. Park, D. Kim, Y. Kim, and B.-J. Yang, *Chin. Phys. B* **28**, 117101 (2019).
- [56] B. Bradlyn, L. Elcoro, J. Cano, M. G. Vergniory, Z. Wang, C. Felser, M. I. Aroyo, and B. A. Bernevig, *Nature (London)* **547**, 298 (2017).
- [57] Bilbao crystallographic server, <http://cryst.ehu.es/cgi-bin/cryst/programs/bandrep.pl>.
- [58] J. P. Provost and G. Vallee, *Commun. Math. Phys.* **76**, 289 (1980).
- [59] T. Neupert, C. Chamon, and C. Mudry, *Phys. Rev. B* **87**, 245103 (2013).
- [60] C. Wu and S.-C. Zhang, *Phys. Rev. B* **71**, 155115 (2005).
- [61] Z.-X. Li, Y.-F. Jiang, and H. Yao, *Phys. Rev. Lett.* **117**, 267002 (2016).
- [62] Z.-X. Li and H. Yao, *Annu. Rev. Condens. Matter Phys.* **10**, 337 (2019).
- [63] J. Hubbard, *Phys. Rev. Lett.* **3**, 77 (1959).
- [64] V. Ambegaokar and M. Troyer, *Am. J. Phys.* **78**, 150 (2010).
- [65] A. Alexandradinata, X. Dai, and B. A. Bernevig, *Phys. Rev. B* **89**, 155114 (2014).
- [66] M. Randeria, N. Trivedi, A. Moreo, and R. T. Scalettar, *Phys. Rev. Lett.* **69**, 2001 (1992).
- [67] N. Trivedi and M. Randeria, *Phys. Rev. Lett.* **75**, 312 (1995).
- [68] P. A. Lee, N. Nagaosa, and X.-G. Wen, *Rev. Mod. Phys.* **78**, 17 (2006).
- [69] V. Peri, Z.-D. Song, M. Serra-Garcia, P. Engeler, R. Queiroz, X. Huang, W. Deng, Z. Liu, B. A. Bernevig, and S. D. Huber, *Science* **367**, 797 (2020).
- [70] Z.-D. Song, L. Elcoro, and B. A. Bernevig, *Science* **367**, 794 (2020).
- [71] S. Liu, A. Vishwanath, and E. Khalaf, *Phys. Rev. X* **9**, 031003 (2019).
- [72] F. N. Únal, A. Bouhon, and R.-J. Slager, *Phys. Rev. Lett.* **125**, 053601 (2020).
- [73] Z.-D. Song, L. Elcoro, Y.-F. Xu, N. Regnault, and B. A. Bernevig, *Phys. Rev. X* **10**, 031001 (2020).
- [74] A. Alexandradinata, J. Höller, C. Wang, H. Cheng, and L. Lu, *Phys. Rev. B* **102**, 115117 (2020).
- [75] M. B. de Paz, M. G. Vergniory, D. Bercioux, A. García-Etxarri, and B. Bradlyn, *Phys. Rev. Research* **1**, 032005 (2019).
- [76] H.-X. Wang, G.-Y. Guo, and J.-H. Jiang, *New J. Phys.* **21**, 093029 (2019).
- [77] K. Latimer and C. Wang, [arXiv:2007.15605](https://arxiv.org/abs/2007.15605) [Phys. Rev. B (to be published)].